Blume-Capel spin-glass model for Fe-Mn-Al alloys

D. Peña Lara,[1,*] J. E. Diosa,[1] and C. A. Lozano[2]
[1]*Departamento de Física, Universidad del Valle, A.A. 25360, Cali, Colombia*
[2]*Grupo de Matemática y Estadística Aplicada, Pontificia Universidad Javeriana, Cali, Colombia*
(Received 30 July 2012; revised manuscript received 28 October 2012; published 5 March 2013)

The spin-glass Blume-Capel model is studied by using an extended mean-field renormalization group approximation. The effects of a probability distribution of the bilinear interaction coupling with competing interactions have been investigated. The phase diagrams show second-order phase boundaries among ferromagnetic, antiferromagnetic, paramagnetic, and spin-glass phases. On the other hand, tricritical phenomena exist only for certain values of the concentration of ferromagnetic bonds as well as ratios of the ferromagnetic to the antiferromagnetic competitive interactions. An application to the magnetic properties of ternary system Fe-Al-Mn alloys is presented. Good fittings to the experimental data are obtained.

DOI: 10.1103/PhysRevE.87.032108 PACS number(s): 75.50.Bb, 75.10.Hk, 64.60.De

I. INTRODUCTION

Fe-Mn-Al disordered alloys have been studied not only to improve their mechanical and magnetic properties but also as possible candidates for corrosion applications and stainless steels [1–3]. These alloys exhibit good oxidation and corrosion resistance and a range of different magnetic phases. Depending on the stoichiometry and temperature treatment, one has ferromagnetic (F), antiferromagnetic (AF), paramagnetic (P), spin-glass (SG), and reentrant spin-glass (RSG) phases [4,5]. These rich properties have been ascribed mainly to the result of (i) the random distribution of their constituent atoms and (ii) the corresponding competing nearest-neighbor interactions coming from different magnetic behavior of the Fe, Mn, and Al atoms.

Theoretical models have been proposed to obtain the phase diagram of this system and to fit some magnetic properties such as the reduced mean hyperfine field at room temperature as a function of Fe, Al, or Mn concentration [6–9]. In general, a spin-1/2 Ising model, with an adequate probability distribution for the exchange interactions, has been used in order to better understand the magnetic behavior of these alloys. The pair approximation based on Bogoliubov's inequality [10] and the mean-field renormalization group approach [11–15] have been applied to get the approximate analytical results.

To explain the magnetic behavior of these alloys, it has been assumed that the aluminum atoms behave as a magnetic hole (thus driving the dilution effect), while the iron and manganese atoms play the role of magnetic sites. Therefore, the theoretical phase diagrams have been obtained within a diluted and random-site Ising model in such a way that good concordance with the experimental data have been achieved by adjusting the Hamiltonian parameters. However, some slight discrepancies have been found in the behavior of the reduced mean hyperfine field as a function of Fe, Al, and Mn concentrations. These disagreements are the subject of the present paper. We believe they can be associated to the magnetic anisotropy, which is present in many magnetic materials. Such an important anisotropy, however, has not been taken into account in the simple Ising models used in previous works.

Recently, an extended spin-1 Ising like system has been introduced in order to study the ternary Fe-Ni-Mn and Fe-Al alloys [16]. The phase diagram for the Fe-Ni-Mn system is in a much better accord with the experimental data than the previous one obtained by using the simple spin-1/2 Ising model, mainly concerning SG and AF phases. The spin-1 model takes into account the electrostatic interactions due to neighboring charges by introducing a parameter called the crystal field (CF) Δ [17]. The CF reduces the degeneracy (since there is no preferred orientation of the angular momentum and, therefore, no preferred orientation of the magnetic moment due to spin) of the electronic levels for two correlated electron spins in zero-field systems (ignoring the electron exchange interaction and only considering the magnetic interactions) with spin $\geqslant 1$ and causes magnetic anisotropy [18,19].

The simplest system that takes in account both physically important terms, namely the exchange interaction and the crystal field, is the so-called Blume-Capel (BC) model [20,21]. The mutual interactions between them ensure the tricritical phenomena, observed, for example, in the metamagnetic system $Ni(NO_3)_2 \cdot 2H_2O$ [22] and in ^{3}He-^{4}He mixtures [23]. At high temperatures the second-order phase transitions are dominated by thermal fluctuations, while at low temperatures the first-order phase transitions occur, beginning from zero temperature ground-state energy crossings. A tricritical point (TCP) separates the high-temperature second-order boundary from the low-temperature first-order boundary. The BC model has been investigated by various techniques, such as the mean-field approximation [24], Monte Carlo simulations [25,26], renormalization group methods [27,28], and conformal invariance [29], among others. In the present case, we study a more general type of competing random-bond BC model, which presents additional spin-glass phases.

In fact, the present work is twofold. First, the disordered Blume-Capel model proposed for these alloys has some interesting thermodynamical properties which have not been, as far as we are concerned, discussed in the literature. Second, we are trying to better understand some experimental anomalies observed in such alloys, which are some decades

*Corresponding author: penalara@univalle.edu.co.

old and with no satisfactory theoretical explanation yet. We believe that with such modeling, new experimental realization for different concentrations of the compounds should be encouraged, mainly in order to seek for the new spin-glass phases predicted by the model.

As we will shortly see, the present model gives indeed a remarkable account for the discrepancies previously obtained for the Fe-Mn-Al alloys by using the spin-1/2 Ising system. Thus, a type of competing diluted and random-bond Blume-Capel model is proposed for the Fe-Mn-Al systems in Sec. II. It is close in spirit but differs from the model proposed for the Fe-Ni-Mn alloys in Ref. [16], mainly regarding the distribution probability of the interactions. In order to treat the continuous transitions of these systems we employ the extended mean-field renormalization group approach that is outlined in Sec. III. The results for the phase diagram by considering a competing probability distribution is presented in Sec. IV, while the application to the Fe-Mn-Al alloys will be discussed in Sec. V. Some final comments and remarks are summarized in Sec. VI. Appendices A and B are devoted to conveying some of the final theoretical expressions for the corresponding physical realizations.

II. RANDOM BLUME-CAPEL MODEL

The Blume-Capel model [20,21] is a simple extension of the spin-1 Ising model for magnetic systems. The Hamiltonian has an additional single site anisotropy factor, or crystal field, and exhibits a second-order phase transition line that joins a first-order transition line at the so-called tricritical point. The Hamiltonian, taking into account random interactions, can be given by

$$H = -\sum_{\langle ij\rangle} J_{ij}\sigma_i\sigma_j + \Delta\sum_{i=1}^{N}\sigma_i^2, \tag{1}$$

where J_{ij} is the random nearest-neighbor bilinear exchange interaction, Δ is the single-ion anisotropy, the first sum is over nearest-neighbor pairs on a lattice of N sites, and the spins σ_i have values $0, \pm 1$.

The random-bond model, which will be applicable to the alloys we have discussed so far, has the following probability distribution [6]:

$$P(J_{ij}) = p\delta(J_{ij} - J) + q\delta(J_{ij}) + x\delta(J_{ij} + \alpha J), \tag{2}$$

where p is the probability of having ferromagnetic bonds J, q for diluted bonds, and x for antiferromagnetic competitive interactions αJ, respectively. We will assume $J > 0$, $\alpha > 0$, and $p + q + x = 1$.

III. THE EXTENDED MFRG APPROACH

The mean-field renormalization group (MFRG) approach [11,12,14] has proven to be efficient and easily applicable in the study of the critical properties of lattice models. The results are satisfactory, even by considering the smallest possibles clusters, namely one spin and a pair of spins. In particular, by using the one- and two-spin clusters in the spin $\sigma = 1/2$ Ising model [11], the critical temperature T_c is equal to that obtained by the Bethe approximation (BA), where the critical exponents are not classic. However, when the same method is applied to the Ising model with $\sigma \geqslant 1$, the results obtained with the smaller clusters are not equivalent to those provided by the BA and, besides, one obtains a critical temperature $T_c \neq 0$ for the one-dimensional model [30,31]. On the other hand, the extended mean-field renormalization (EMFRG) approach gives, for the smallest cluster, the same results for T_c as those obtained from BA and constant coupling approximation [10] as well for the quadrupole moment $Q = \langle\sigma^2\rangle$.

To illustrate the application of the EMFRG approach, we will take herein the smallest clusters and consider the ferromagnetic phase first. Thus, the Hamiltonian for the one-spin cluster ($N' = 1$) is

$$H_1 = -zJ'b'\sigma_1 - z\gamma_1\sigma_1^2 + \Delta'\sigma_1^2, \tag{3}$$

where z is the coordination number of the lattice. b' is the symmetry breaking boundary condition acting at the boundary of the cluster and is related to the ferromagnetic order parameter of the system ($\langle\sigma\rangle$). γ_1 is an additional parameter related to the mean square of the spin ($\langle\sigma^2\rangle$).

Similarly, for the two-spin cluster ($N = 2$), one has

$$\begin{aligned} H_2 = &-J_{12}\sigma_1\sigma_2 - (z-1)J_1b_1\sigma_1 - (z-1)J_2b_2\sigma_2 \\ &+ (z-1)\gamma_2\left(\sigma_1^2 + \sigma_2^2\right) + \Delta\left(\sigma_1^2 + \sigma_2^2\right), \end{aligned} \tag{4}$$

where b_i, $i = 1,2$, and γ_2 have the same meanings as above.

For these clusters we have

$$m_1 = \frac{e^{\delta_1}\sinh(I_0)}{1 + 2e^{\delta_1}\cosh(I_0)}, \tag{5}$$

$$Q_1 = \frac{e^{\delta_1}\cosh(I_0)}{1 + 2e^{\delta_1}\cosh(I_0)}, \tag{6}$$

where $I_0 = zK'b'$, $K' = \beta J'$, $\beta = (k_BT)^{-1}$, k_B is the Boltzmann constant, and $\delta_1 = z\beta\gamma_1 - \beta\Delta' \equiv q_1 - D'$. $m_1 = \langle\sigma_1\rangle_1$ and $Q_1 = \langle\sigma_1^2\rangle_1$ are the mean values related to the one-spin cluster and

$$\begin{aligned} m_2 = &e^{\delta_2}\{\sinh(I_1) + e^{\delta_2+K_{12}}\sinh(I_1 + I_2) \\ &+ e^{\delta_2-K_{12}}\sinh(I_1 - I_2)\}/Z_2, \end{aligned} \tag{7}$$

$$\begin{aligned} Q_2 = &e^{\delta_2}\{\cosh(I_1) + \cosh(I_2) + 2e^{\delta_2+K_{12}}\cosh(I_1 + I_2) \\ &+ e^{\delta_2-K_{12}}\cosh(I_1 - I_2)\}/Z_2, \end{aligned} \tag{8}$$

with

$$\begin{aligned} Z_2 = &1 + 2e^{\delta_2}\cosh(I_1) + 2\cosh(I_2) \\ &+ 2e^{\delta_2+K_{12}}\cosh(I_1 + I_2) + e^{\delta_2-K_{12}}\cosh(I_1 - I_2), \end{aligned}$$

where $I_i = (z-1)K_ib_i$, $K_i = \beta J_i$, and $\delta_2 = (z-1)\beta\gamma_2 - \beta\Delta \equiv q_2 - D$. $m_2 = \langle\sigma_1\rangle_2, Q_1 = \langle\sigma_1^2\rangle_2$ are the mean values related to the two-spin cluster.

A. Obtaining the critical line

Close to a critical transition the magnetization is very small and, assuming that $b' \ll 1$ and $b \ll 1$ (where $b_1 = b_2 = b$ in the ferromagnetic case), we can expand to third order in b' and

b, respectively, to obtain

$$m_1 = f_1(K',D',q_1)b' + g_1(K',D',q_1)b'^3, \quad (9)$$

$$Q_1 = h_1(K',D',q_1), \quad (10)$$

$$m_2 = f_2(K,D,q_2)b + g_2[K,D,q_2)b^3, \quad (11)$$

$$Q_2 = h_2(K,D,q_2). \quad (12)$$

Expressions for f_i, g_i and $h_i, i = 1,2$ are given in Appendix A.

The critical properties of the system are obtained by assuming that Eqs. (9) and (11) scale as

$$m_1 = \ell^{d-y_H} m_2, \quad (13)$$

and imposing a same scaling relation for b' and b, i.e.,

$$b' = \ell^{d-y_H} b, \quad (14)$$

where $\ell = (N/N')^{1/d}$ is the scaling factor, d is the dimension of the lattice, and y_H is the magnetic critical exponent. From Eqs (5), (7), (13), and (14) we obtain

$$f_1(K',D',q_1) = f_2(K,D,q_2), \quad (15)$$

which is independent of any scaling factor and can be viewed as a renormalization recursion relation among the parameters of the Hamiltonian. When $q_1 = q_2 = 0$ and $\sigma = 1$, Eq. (15) has the same functional form of Eq. (7) obtained in Ref. [30], which has a nonzero transition temperature for the one-dimensional model.

From Eq. (15) is not possible to determine a complete renormalization group flow in the parameter space; therefore, the critical properties can be analyzed by restricting the space to the physical plausible invariant subset $D' = D$ [16]. Note that the quantity $Q = \langle\sigma^2\rangle$ is not critical as the magnetization. In this sense, its anomalous dimension is zero, so we can assume $Q_1 = Q_2 = Q$ and impose the same relation for the parameters q_1 and q_2, i.e., $q_1 = q_2 = q$. Thus, Eq. (15) becomes

$$f_1(K',D,q) = f_2(K,D,q) \quad (16)$$

and from Eqs. (10) and (12) we get

$$h_1(K',D,q) = h_2(K,D,q). \quad (17)$$

Equations (16) and (17) give the fixed point $K' = K = K_c$. In this way, besides the critical temperature and the thermal critical exponent, one is also able to obtain a thermodynamical property (equation of state), in this case $\langle\sigma^2\rangle$, which is not usual in the MFRG approach for $\sigma = 1/2$ models.

For the antiferromagnetic phase the calculations are quite similar. One has to consider two sublattices with opposite magnetizations, where $b_1 = -b_2 = b$. In doing so, the critical behavior happens to be exactly the same as that developed above for the ferromagnetic case, with the sublattice magnetization playing the role of the order parameter.

B. Location of the tricritical point

The MFRG approach locates the TCP by obtaining the critical temperature T_c as a function of the parameter D. In general, we have a point (D_T, T_T), where $(dT_c/dD)_T \to \infty$ such that for $D > D_T$ there is no solution for T_c while for $D < D_T$ there are two solutions for T_c. This special point is associated to TCP, but there is an ambiguity to distinguish a TCP and a possible second-order reentrancy in the phase diagram of the model. The idea is to explore the cubic term in Eqs. (9) and (11) and from Eq. (16) we have an additional equation,

$$g_1(K,D,q) = g_2(K,D,q). \quad (18)$$

When Eq. (18) is satisfied, TCP is located without ambiguity. Thus, the second-order transitions and the location of the TCP are identical to those obtained by a Landau expansion in the free energy of the model.

C. Obtaining the spin-glass phase transition

Spin glass is observed in a variety of disordered magnetic materials and involving both competing J_{ij} and disorder. Due to the randomness of the interactions J_{ij}, we expect the average magnetization to vanish. However, averages involving squares of the magnetization are generally nonzero. Spin glasses are described by the Edwards-Anderson order parameter $q_{EA} = \overline{\langle\sigma\rangle^2}$, where the brackets mean the thermal average and the overline means the configurational average over the random bonds [32]. By following the same procedure above one gets for the spin-glass order parameter

$$q_{EA1}(K',D,q,b') = j_1(K',D,q)b'^2, \quad (19)$$

$$q_{EA2}(K,D,q,b) = j_2(K,D,q)b^2. \quad (20)$$

Assuming a similar scaling relation $q_{EA1} = \ell^\theta q_{EA2}$ and $b'^2 = \ell^\theta b^2$, where θ is the anomalous dimension of the spin-glass order parameter, we have

$$q_{EA1}(K',D,q) = q_{EA1}(K,D,q). \quad (21)$$

Accordingly, we can also compute the noncritical variable $R = \overline{\langle\sigma^2\rangle^2}$, from which we arrive at the relation

$$R_1(K',D,q,b'^2 = 0) = R_2(K,D,q,b^2 = 0). \quad (22)$$

From Eqs. (21) and (22) we get the spin-glass transition line.

IV. GENERAL OVERVIEW OF THE PHASE DIAGRAMS

Before discussing the experimental realization of the ternary alloys it is worthwhile to get a picture of the phase diagrams of the present models as a function of its theoretical parameters.

Figure 1(a) shows the reduced critical temperature ($\tau \equiv k_B T/J$) as a function of the reduced crystal field ($\delta \equiv \Delta/J$) for various values of the antiferrromagnetic interaction concentration (x) for lattice coordination number $z = 8$ and parameter $\alpha = 1$. For $q = 0$ and $x > 0.3$, the tricritical phenomenon is not more present. Table I reports some values for δ_T and τ_T for different concentrations x. The localization of TCP is given when Eq. (18) is satisfied along the second-order transition line. For $p = 1$ (or $q = 0$ and $x = 0$), we recover the previous phase diagram of the spin-1 Blume-Capel model according to the extended MFRG [33]. For the cases when $q = 0$ with $x = 0$ (yellow line), $x = 0.10$ (orange line), $x = 0.20$ (wine line),

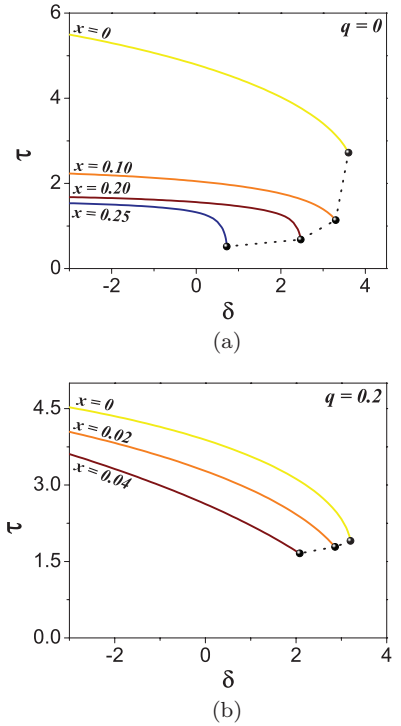

FIG. 1. (Color online) Phase diagram in the reduced crystal field ($\delta \equiv \Delta/J$) and the reduced critical temperature ($\tau \equiv k_B T/J$) plane for various antiferromagnetic concentrations x. (a) For $q = 0$ with $x = 0$ (yellow line), $x = 0.10$ (orange line), $x = 0.20$ (wine line), and $x = 0.25$ (blue line). (b) For $q = 0.2$ with $x = 0$ (yellow line), $x = 0.02$ (orange line), and $x = 0.04$ (wine line). The dotted line corresponds to TCPs. For this case $\alpha = 1$ and $z = 8$.

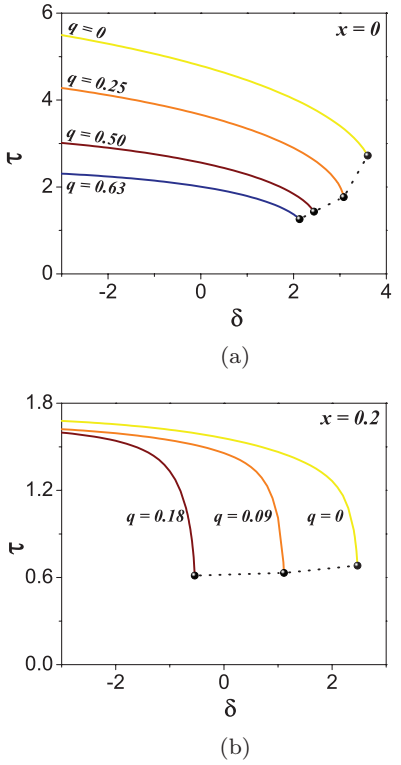

FIG. 2. (Color online) The same as described in the caption to Fig. 1 for several dilution concentrations (q) in the δ,τ plane for (a) $x = 0$ with $q = 0$ (yellow line), $q = 0.25$ (orange line), $q = 0.50$ (wine line), and $q = 0.63$ (blue line). For (b) $x = 0.2$ with $q = 0$ (yellow line), $q = 0.09$ (orange line), and 0.18 (wine line).

and $x = 0.25$ (blue line), the behavior of $\delta = \delta(\tau)$ is similar to that of Fig. 1 reported in Ref. [16]. For this case, τ decreases when δ decreases up to $\delta_T = 0.72$ and $\tau_T = 0.517$; below this pair of values the tricritical behavior is suppressed. For the particular range $0.20 < x < 0.25$, the temperature presents a more pronounced decay behavior and one reason may be the strong competition between the parameters involved, namely δ, τ, and q. Similar behavior is found for $q = 0.2$ and $x = 0$ (yellow line), $x = 0.02$ (orange line), and $x = 0.04$ (wine line), as shown in Fig. 1(b) and Table I. Here, for antiferrromagnetic interaction concentrations $x > 0.04$ the tricritical phenomenon disappears.

In Fig. 2(a) we have the corresponding phase diagrams from $q = 0$ (yellow line), $q = 0.25$ (orange line), $q = 0.50$ (wine line), and $q = 0.63$ (blue line) for $x = 0$, whose behavior is similar to Fig. 1(b), but in this case we have a wider range for q where the tricritical phenomenon is observed. However, for $x = 0.2$ with $q = 0$ (yellow line), $q = 0.09$ (orange line), and 0.18 (wine line), the curves present a stronger decay to the TCP. Table II shows the values for tricritical points obtained according to Eq. (18). In both Figs. 1 and 2 above the transitions are from the ferromagnetic ordered phase to the paramagnetic disordered phase.

On the other hand, the phase diagrams on the space of reduced temperature (τ) and concentration of antiferromagnetic bonds (x), for various reduced (positive and negative) crystal fields (δ), present a second-order transition line that decreases with the decreasing of x and goes to zero at a critical value x_c. As the system is rich in antiferromagnetic bonds, the transition is from the antiferromagnetic ordered phase to the disordered

TABLE I. Values of the tricritical points δ_T, τ_T for different x and fixed q concentrations.

q	x	δ_T	τ_T
	0	3.60	2.724
	0.1	3.30	1.139
0	0.2	2.47	0.682
	0.3	0.72	0.517
	0	3.20	1.904
0.2	0.02	2.86	1.785
	0.04	2.08	1.659

TABLE II. Values of the tricritical points (δ_T, τ_T) for different q and fixed x concentrations.

x	q	δ_T	τ_T
	0	3.60	2.723
0	0.25	3.08	1.766
	0.50	2.44	1.433
	0.65	2.13	1.261
	0	2.47	0.682
0.20	0.99	1.11	0.631
	0.18	−0.54	0.613

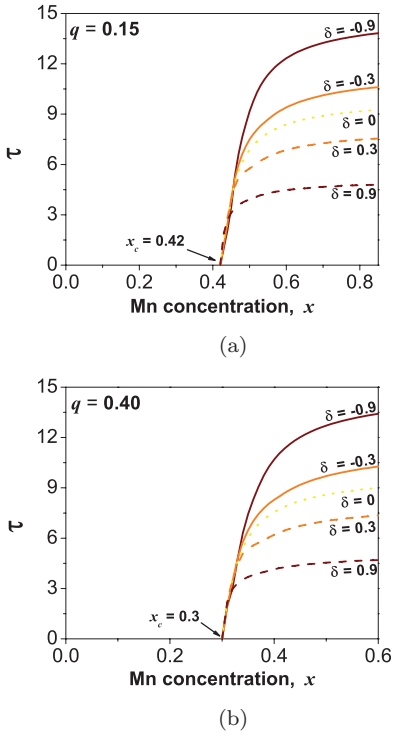

FIG. 3. (Color online) Reduced critical temperature as function of the concentration of antiferromagnetic bonds for different crystal fields δ and $z = 8$. (a) For $q = 0.15$ with $\delta = -0.9$ (wine line), $\delta = -0.3$ (orange line), $\delta = 0$ (yellow dot line), $\delta = 0.3$ (orange dashed line), and $\delta = 0.9$ (wine dashed line), we have $x_c = 0.42$. (b) For $q = 0.40$ with $\delta = -0.9$ (wine line), $\delta = -0.3$ (orange line), $\delta = 0$ (yellow dot line), $\delta = 0.3$ (orange dashed line), and $\delta = 0.9$ (wine dashed line), we have $x_c = 0.30$.

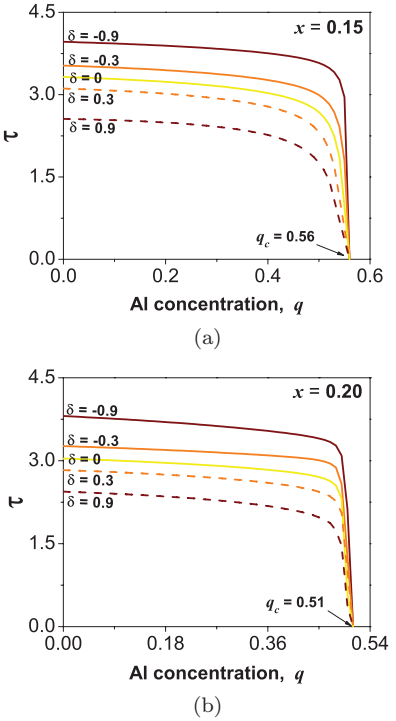

FIG. 4. (Color online) The same as described in the captin to Fig. 3 for several concentrations. (a) $x = 0.15$ with $q_c = 0.56$. (b) $x = 0.20$ and we have $q_c = 0.51$.

paramagnetic phase. That is why the temperature reduces as x decreases. For instance, at $q = 0.15$, Fig. 3(a) shows a value $x_c = 0.42$ and for $q = 0.40$ the corresponding value is $x_c = 0.30$, as is shown in Fig. 3(b). Both figures have a similar behavior. The competition between q and δ is more evident.

For $x = 0.15$ with $\delta = -0.9$ (wine line), $\delta = -0.3$ (orange line), $\delta = 0$ (yellow dot line), $\delta = 0.3$ (orange dashed line), and $x = 0.20$ with $\delta = -0.9$ (wine line), $\delta = -0.3$ (orange line), $\delta = 0$ (yellow dot line), $\delta = 0.3$ (orange dashed line), a similar behavior is found as a function of q. In this case, τ decreases as q increases until it reaches the critical value for $q_c = 0.56$ for $x = 0.15$ [as shown in Fig. 4(a)] and $q_c = 0.51$ for $x = 0.20$ [as shown in Fig. 4(b)]. As before, in both cases the negative δ values are slightly above the positive ones. Here the transition is from the ferromagnetic to the paramagnetic phases.

The quadrupolar quantity Q as a function of δ along the transition line for some x values ($x = 0$ yellow line and $x = 1.0$ orange line) with q constant (=0) is shown in Fig. 5(a). This is in fact an equation of state which has been obtained from the EMFRG approach [27] for $p = 1$ or $x = 0$. In this work and for $x = 0$, Q decreases from negative to positive values of δ until $\delta_c \approx 2.0$, where $Q = 0$, and for the case $x = 1.0$, Q begins above $x = 0$ but ends in the same value $\delta_c \approx 2.0$, in contrast to what was found in Ref. [27], where the curve tends to zero. Similar behavior can viewed in Fig. 5(b) where q has a range between 0 (yellow line) to 0.99 (orange line) and the Q-initial values are lower. A detailed analysis of the low-temperature region of the phase diagram presenting first-order transitions is not possible by using the EMFRG because it treats only second-order phase transitions.

A global theoretical phase diagram in the p-τ plane for coordination number $z = 8$, $\alpha = 1$, and $\delta = 1$ with $q = 0$ (yellow line) and $q = 0.1$ (orange dot line) is shown in Fig. 6(a), and for $\delta = -1$ with $q = 0$ (yellow line) and $q = 0.1$ (orange dot line) in Fig. 6(b), according to the probability distribution (2). In particular, when $\delta \to -\infty$ we recover the Fig. 1 of Ref. [6]. Both figures exhibit a similar behavior for positive or negative δ values and a nonsymmetric phase diagrams is obtained, in disagreement with Ref. [6]. For $q = 0$, the ferromagnetic boundary decreases as p decreases until near the critical Fe concentration, tending then abruptly to zero. The antiferromagnetic boundary remains almost constant with p until very near the critical Fe concentration, and again tends to zero abruptly. The spin-glass transition temperature continues being independent of the ferromagnetic bond concentration for a fixed q. For $q = 0.1$ the behavior is similar but shifts to the left, as shown in Fig. 6(a). For negative δ values, the phase diagram is similar to that in Fig. 6(a); however, the paramagnetic boundary is slightly wider and the ferromagnetic boundary now is constant as p decreases, as shown in Fig. 6(b). The critical Fe concentration is given by $p_c^+ \approx \frac{z(3-q)}{2(3z-2)}$ for positive values of the reduce crystal field δ. This behavior is observed in the experimental realization $Fe_xMn_{0.600-x}Al_{0.400}$, $0.200 \leqslant x \leqslant 0.600$ [34]. For positive values of δ, we have a similar behavior as in Fig. 6(a), but in this case the F and AF boundaries increase when q increases; the critical value for p is reached in this case at $p_c^- \approx \frac{z(3-q)}{2(3z-1)}$.

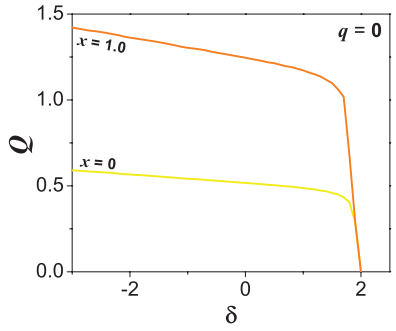

(a)

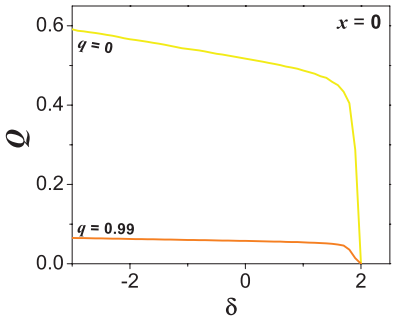

(b)

FIG. 5. (Color online) Quadrupolar quantity (Q) as a function of δ along the transition line. (a) $q = 0$ with $x = 0$ (yellow line) and $x = 1.0$ (orange line). (b) $x = 0$ with $q = 0$ (yellow line) and $q = 0.99$ (orange line).

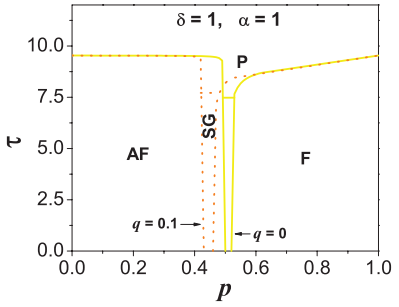

(a)

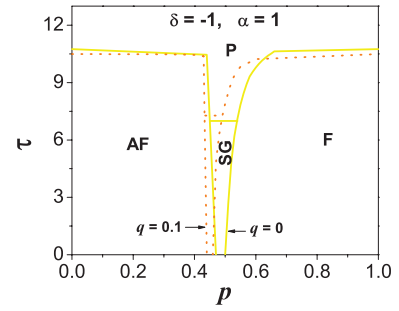

(b)

FIG. 6. (Color online) Nonsymmetric random-bond phase diagram for different values of q, $\alpha = 1$, and two values (positive and negative) of δ: (a) $\delta = 1$ with $q = 0$ (yellow line) and $q = 0.1$ (orange dot line); (b) $\delta = -1$ with $q = 0$ (yellow line) and $q = 0.1$ (orange dot line). Phases are abbreviated as follows: antiferromagnetic (AF), ferromagnetic (F), paramagnetic (P), and spinglass (SG).

V. APPLICATION TO THE FE-MN-AL TERNARY ALLOYS

The phase diagram of the Fe-Mn-Al ternary alloys shows several phases which depend on the atomic percentage of iron, manganese, and aluminum atoms. Thus, for example, we found spin-glass (SG) and reentrant spin-glass (RSG) behavior, as a consequence of the presence of competing ferromagnetic (Fe-Fe) and antiferromagnetic (Fe-Mn) interactions [35]. These ternary Fe-Mn-Al systems are also a good candidate to replace the conventional stainless steel. Thus, from a theoretical viewpoint, they are quite attractive regarding their physical and mechanical properties, too [36]. In this section we will discuss the application of the present theoretical model to the magnetic properties of these ternary alloys. In Ref. [6] it was used a diluted and random-bond Ising model where it was assumed that the Mn atom behaves as Al atoms with the Fe magnetic moment constant and the Al atoms behaving like magnetic holes. This is true for small Mn concentrations (x), but when we have large Mn concentrations, an antiferromagnetic interaction is induced. For $x = 0$, the site and bond-dilute Ising model explain the observed behavior. But for $x \neq 0$ one can also assume $\alpha = x$, i.e., enhancing the AF interaction as the Mn concentration is increased. We also consider, as given in Ref. [6], that the exchange parameter J depends on q and is independent of x, namely $J(q) = J_1 - qJ_0$. The values for the theoretical parameters $J_1 = 12.846$ meV and $J_0/J_1 = 0.95$ used in Ref. [6] are the same in the present study, and the value for δ which gives the best results is chosen to be 1.5.

In order to apply the spin-glass Blume-Capel model to these alloys we will use the pair approximation based on Bogoliubov's inequality [10] to compute the ferromagnetic order parameter $\langle\overline{\sigma}\rangle \equiv m \propto \overline{H}$, where $\overline{H}$ is the mean reduced hyperfine field. The procedure is similar to that performed in Ref. [16], and Appendix B gives the equations to be solved by use of numerical methods. The solid line in Fig. 7 was obtained from the present model and the dashed line represents the theoretical fitting from the previous simple Ising model. This figure shows the behavior of the mean reduced hyperfine field (H) as function of Mn concentration (x) for various Al concentrations (q). It can be observed that with the present model, considering the probability distribution (2), and the same adjusted values of J_1 and J_0/J_1, better fittings are obtained in comparison with those of Ref. [6]. The interaction between δ, J and the corresponding equation $J(q) = J_1 - qJ_0$ gives a better agreement between the experimental and theoretical data. Similar results are depicted in Fig. 8, where we have the behavior between $\overline{H}$ as a function of Mn concentration.

VI. CONCLUSIONS AND REMARKS

In summary, the thermodynamical behavior of the ternary Fe-Mn-Al system was described through an approximate scheme by taking the pair approximation based on Bogoliubov inequality. The agreement achieved from the present approach is far better than the previous one by taking a simple Ising model. For this system we assumed that Fe atoms interact ferromagnetically, Mn atoms behave with antiferromagnetic interactions, and Al atoms are paramagnetic. Therefore, according to the Bethe-Slater curve these alloys are in fact

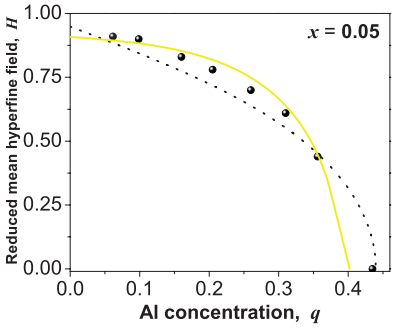

(a)

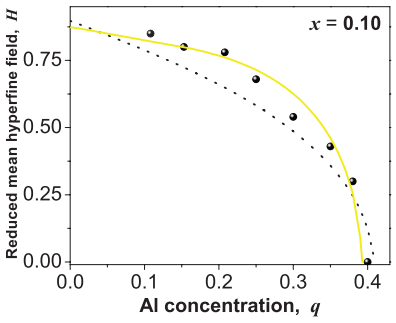

(b)

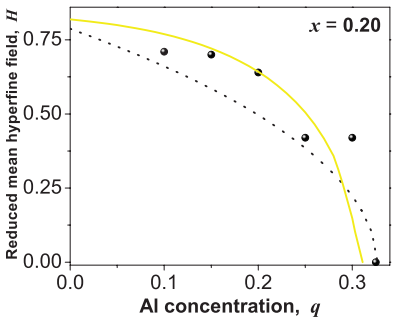

(c)

FIG. 7. (Color online) Mean hyperfine field H as function of Al concentration q for different values of x. (a) $x = 0.05$, (b) $x = 0.10$, and (c) $x = 0.20$. The experimental results (dots) were fitted by the model discussed in Ref. [6] (black dashed line) and the yellow solid line represents the theoretical results according to the present model.

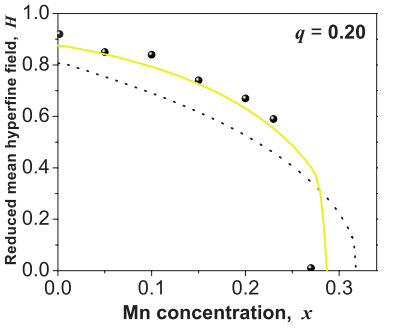

(a)

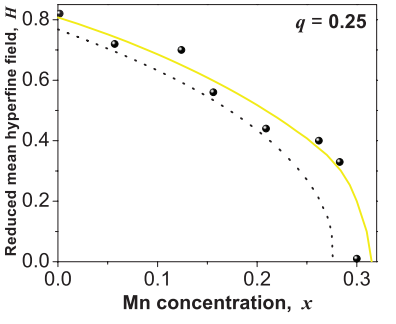

(b)

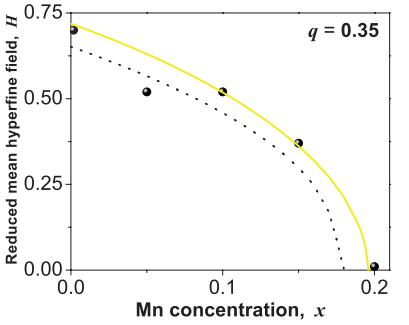

(c)

FIG. 8. (Color online) Mean hyperfine field H as function of Mn concentration x for different values of q. (a) $q = 0.20$, (b) $q = 0.25$, and (c) $q = 0.35$. The experimental results (dots) were fitted by the model discussed in Ref. [6] (black dashed line) and the yellow solid line represents the theoretical results according to the present model.

a prototype to be described by the Blume-Capel model with the appropriate diluted and random-bond distribution (2). The theoretical phase diagrams obtained for the positive values of the reduced crystal field present qualitatively the same behavior as the experimental data reported in the literature for the system $Fe_xMn_{0.600-x}Al_{0.400}$, $0.200 \leqslant x \leqslant 0.600$, which will be applied to the present model in a future work. This system presents several phases as ferro, antiferro, para, spin glass, reentrant spin glass, superparamagnetism, and so on. It should be stressed that a similar spin-1 model has been recently applied to the binary Fe-Al compound [37,38] with results that are not much improved when compared to the spin-1/2 counterpart [39]. Despite that, we believe that the anisotropy present in these experimental realizations is in fact important and should be well described by models with spin greater than 1/2. In addition, as the spin-glass region is dependent on the the crystal field, it should be very welcome to have new experimental realizations with different crystal field interactions in order to seek the differences of the corresponding spin-glass region in the phase diagram.

ACKNOWLEDGMENTS

One of the authors (D.P.L.) thanks the Research Vice Chancellor of Universidad del Valle for funding (Grant No.7905).

APPENDIX A: EQUATIONS FOR EMFRG

In this Appendix we present the analytical results leading to the second-order ferromagnetic transition line as well as the Edwards-Anderson spin-glass transition line for the random-bond distribution (2).

In what follows we have

$$K = \beta J \qquad \beta = \frac{1}{k_B T}$$

$$\delta = \frac{\Delta}{J} \qquad \delta_1 = zg - \delta$$

$$\delta_2 = [(z-1)g - \delta]K \qquad I_0 = zK_i' b_i'$$

$$I_1 = (z-1)K_1 b_1 \qquad I_2 = (z-1)K_2 b_2$$

$$Z_1(K') = 1 + 2e^{\delta_1 K'}, \tag{A1a}$$

$$Z_2(K_i) = 1 + 4e^{\delta_2}\{1 + e^{\delta_2}\cosh(K_i)\}. \tag{A1b}$$

For the magnetizations (F/AF and first/third order) and quadrupoles we obtain [$\kappa = (z-1)e^{\delta_2}$]

$$m_{1,f} = z\left[\frac{q}{Z_1(0)} + \frac{pe^{\delta_1 K}}{Z_1(K)} + \frac{xe^{-\alpha\delta_1 K}}{Z_1(-\alpha K)}\right], \tag{A2a}$$

$$m_{2,f} = \kappa\left[\frac{q}{Z_2(0)} + \frac{pW_1^+(K)}{Z_2(K)} + \frac{xW_1^-(-\alpha K)}{Z_2(\alpha K)}\right], \tag{A2b}$$

$$m_{1,t} = \frac{z^3}{6}\left[\frac{q}{Z_1(0)} + \frac{pW_2(K)}{Z_1^2(K)} + \frac{xW_2(\alpha K)}{Z_1^2(-\alpha K)}\right], \tag{A2c}$$

$$m_{2,t} = \kappa^3\left[\frac{qW_3}{Z_2(0)} + \frac{pW_4(K)}{Z_2(K)} + \frac{xW_4(\alpha K)}{Z_2(\alpha K)}\right]. \tag{A2d}$$

$$Q_1 = \frac{q}{Z_1(0)} + \frac{pe^{\delta_1 K}}{Z_1(K)} + \frac{xe^{-\alpha\delta_1 K}}{Z_1(-\alpha K)}, \tag{A3a}$$

$$Q_2 = e^{\delta_2}\left[\frac{q}{Z_2(0)} + \frac{pW_5(K)}{Z_2(K)} + \frac{xW_5(\alpha K)}{Z_2(\alpha K)}\right], \tag{A3b}$$

where

$$W_1^{\pm}(K_i) = 1 + 2e^{\delta_2}\cosh(K_i) \pm 2e^{\delta_2}\sinh(K_i),$$

$$W_2(K') = e^{\delta_1 K'}(4e^{\delta_1 K'} - 1),$$

$$W_3 = 4e^{\delta_2} - 1,$$

$$W_4(K_i) = 2e^{\delta_2} - 1 + 2e^{\delta_2}(6e^{\delta_2} - 1)\cosh(K_i) + 16e^{3\delta_2}\cosh^2(K_i),$$

$$W_5(K_i) = 1 + 2e^{\delta_2}\cosh(K_i).$$

For the Edwards-Anderson spin-glass parameter we get

$$n_1 = z^2\left[\frac{q}{Z_1^2(0)} + \frac{pe^{2\delta_1 K}}{Z_1^2(K)} + \frac{xe^{-2\alpha\delta_1 K}}{Z_1^2(\alpha K)}\right], \tag{A4a}$$

$$n_2 = \kappa^2\left[\frac{q}{Z_2^2(0)} + \frac{pW_6(K)}{Z_2^2(K)} + \frac{xW_6(\alpha K)}{Z_2^2(\alpha K)}\right], \tag{A4b}$$

$$R_1 = \frac{q}{Z_1^2(0)} + \frac{pe^{2\delta_1 K}}{Z_1^2(K)} + \frac{xe^{-2\alpha\delta_1 K}}{Z_1^2(\alpha K)}, \tag{A4c}$$

$$R_2 = e^{\delta_2}\left[\frac{q}{Z_2(0)} + \frac{pW_7(K)}{Z_2(K)} + \frac{xW_7(\alpha K)}{Z_2(\alpha K)}\right], \tag{A4d}$$

where

$$W_6(K_i) = 1 + 4e^{\delta_2}\cosh(K_i) + 4e^{2\delta_2}\cosh(2K_i),$$

$$W_7(K_i) = \{1 + 2e^{\delta_2}\cosh(K_i)\}^2.$$

APPENDIX B: EQUATIONS FOR THE PAIR APPROXIMATION

The pair approximation based on the Bogoliubov inequality for the free energy [10] follows closely the procedure used in Ref. [16]. We introduce the notation:

$$r = \frac{z-1}{z} \qquad d = \beta\Delta,$$

$$a = \beta\gamma_1 \qquad b = \beta\gamma_2$$

Magnetization:

$$m_s = \frac{e^{b-d}\sinh(a)}{1 + 2e^{b-d}\cosh(a)}, \tag{B1}$$

$$m_p = \frac{qW_8(0)}{Z_p(0)} + \frac{pW_8(K)}{Z_p(K)} + \frac{xW_8(-\alpha K)}{Z_p(-\alpha K)}. \tag{B2}$$

Quadrupole:

$$Q_s = \frac{e^{b-d}\cosh(a)}{1 + 2e^{b-d}\cosh(a)} \tag{B3}$$

$$Q_p = \frac{qW_9(0)}{Z_p(0)} + \frac{pW_9(K)}{Z_p(K)} + \frac{xW_9(-\alpha K)}{Z_p(-\alpha K)}$$

where

$$Z_p(K') = 1 + 2e^{2(rb-d)+K'} + 4e^{rb-d}\cosh(ra) + 2e^{2(rb-d-K')}\cosh(2ra) \tag{B4}$$

and with

$$W_8(K') = e^{rb-d}[\sinh(ra) + e^{rb-d+K'}\sinh(2ra)]$$

$$W_9(K') = e^{rb-d}[e^{rb-d} + \cosh(ra) + e^{rb-d+K'}\cosh(2ra)]$$

The above procedure has been done for the ferromagnetic model. Nevertheless, the same equations are obtained for the antiferromagnetic case, where m_1 and m_2 are treated as sublattice magnetizations.

[1] G. L. Kayak, Met. Sci. Heat Treat. **2**, 95 (1969).

[2] P. D. Bilmes, A. C. González, C. L. Llorente, and M. Cuyás y Solari, Rev. Metal. Madrid **30**, 298 (1994).

[3] K. Tarigan, IEEE Trans. Magn. **45**, 2492 (2009).

[4] G. A. Pérez Alcázar, J. A. Plascak, and E. Galvão da Silva, Phys. Rev. B **38**, 2816 (1988).

[5] T. V. S. M. Mohan Babu and C. Bansal, Phys. Status Solidi B **193**, 167 (1996).

[6] A. Rosales Rivera, G. A. Pérez Alcázar, and J. A. Plascak, Phys. Rev. B **41**, 4774 (1990).
[7] Ligia E. Zamora, G. A. Pérez Alcázar, A. Bohorquez, A. Rosales Rivera, and J. A. Plascak, Phys. Rev. B **51**, 9329 (1995).
[8] Ligia E. Zamora, G. A. Pérez Alcázar, C. González, J. M. Greneche, W. R. Aguirre, A. Bohórquez, E. M. Baggio Saitovich, and D. Sánchez, J. Magn. Magn. Mater. **301**, 495 (2006).
[9] E. A. Velásquez, L. F. Duque, J. Mazo-Zuluaga, and J. Restrepo, Physica B **398**, 364 (2007).
[10] L. G. Ferreira, S. R. Salinas, and M. J. Oliveira, Phys. Status Solidi B **83**, 229 (1977).
[11] J. O. Indekeu, A. Maritan, and A. L. Stella, J. Phys. A **15**, L291 (1982).
[12] J. O. Indekeu, A. Maritan, and A. L. Stella, Phys. Rev. B **35**, 305 (1987).
[13] M. Droz, A. Maritan, and A. L. Stella, Phys. Lett. A **92**, 287 (1982).
[14] J. A. Plascak, W. Figueiredo, and B. C. S. Grandi, Braz. J. Phys. **29**, 579 (1999).
[15] M. L. Lyra and S. Coutinho, Physica A **155**, 232 (1989).
[16] D. Peña Lara, G. A. Pérez Alcázar, Ligia E. Zamora, and J. A. Plascak, Phys. Rev. B **80**, 014427 (2009).
[17] J. H. Van Vleck, *The Theory of Electric and Magnetic Susceptibilities* (Oxford University Press, New York, 1932).
[18] R. M. Bozorth, *Ferromagnetism* (IEEE, Inc., New York, 1978).
[19] R. C. Ohandley, *Modern Magnetic Materials: Principles and Applications* (John Wiley & Sons, New York, 2000).
[20] M. Blume, Phys. Rev. **141**, 517 (1966).
[21] H. W. Capel, Physica **32**, 966 (1966).
[22] V. A. Schmidt and S. A. Friedberg, Phys. Rev. B **1**, 2250 (1970).
[23] M. Blume, V. J. Emery, and R. B. Griffths, Phys. Rev. A **4**, 1071 (1971).
[24] J. A. Plascak, J. G. Moreira, and F. C. Sá Barreto, Phys. Lett. A **173**, 360 (1993).
[25] A. K. Jain and D. P. Landau, Phys. Rev. B **22**, 445 (1980).
[26] C. J. Silva, A. A. Caparica, and J. A. Plascak, Phys. Rev. E **73**, 036702 (2006).
[27] D. Peña Lara and J. A. Plascak, Mod. Phys. Lett. B **10**, 1067 (1996).
[28] D. Peña Lara and J. A. Plascak, Int. J. Mod. Phys. **12**, 2045 (1998).
[29] J. C. Xavier, F. C. Alcaraz, D. Peña Lara, and J. A. Plascak, Phys. Rev. B **57**, 11575 (1998).
[30] O. F. de Alcantara Bonfim, Physica A **130**, 367 (1985).
[31] W. Figueiredo and B. C. S. Grandi, Braz. J. Phys. **30**, 58 (2000).
[32] R. Skomski, *Simple Models of Magnetism* (Oxford University Press, Oxford, 2008).
[33] D. Peña Lara, J. A. Plascak, and J. Ricardo de Souza, Int. J. Mod. Phys. B **12**, 1813 (1998).
[34] Claudia González, G. A. Pérez Alcázar, Ligia E. Zamora, Jesús A. Tabares, and Jean-Marc Greeneche, J. Phys.: Condens. Matter **14**, 6531 (2002).
[35] V. Raghavan, J. Phas. Equi. Diff. **26**, 65 (2005).
[36] MAJ R. A. Howell, Ph.D. thesis, Missouri University of Science and Technology, 2011.
[37] D. A. Dias, J. Ricardo de Sousa, and J. A. Plascak, Phys. Lett. A **373**, 3513 (2009).
[38] D. A. Dias and J. A. Plascak, Phys. Lett. A **375**, 2089 (2011).
[39] A. S. Freitas, D. F. de Albuquerque, and N. O. Moreno, Physica A **391**, 6332 (2012).